SER Compliance of WCAP-12610-P-A & CENPD-404-P-A Addendum 1-A "Optimized ZIRLO™" (Non-Proprietary)

February 2013

Westinghouse Electric Company LLC
1000 Westinghouse Drive
Cranberry Township, PA 16066

Executive Summary

This report provides additional information from irradiation programs in compliance with NRC Conditions 6 and 7 of Section 5.0 of the SER to the **Optimized ZIRLO™*** topical report WCAP-12610-P-A & CENPD-404-P-A Addendum 1-A (Reference 1).

Visual observations and measurements of oxidation of fuel rods, fuel rod length, and fuel assembly length data are provided as required by Condition 6 for **Optimized ZIRLO** LTAs. The additional data continues to confirm the applicability of currently approved fuel performance models for **Optimized ZIRLO** material. Irradiation creep and irradiation growth data from the once-burned and twice-burned Vogtle Creep/Growth tests are consistent and repeatable with respect to the more recent data obtained at the end of the third burn. Irradiation creep of PRXA **Optimized ZIRLO** material is shown to be comparable to Standard ZIRLO®* material and the stress dependence of the irradiation creep strain is linear. The steady state irradiation creep strains in tension and in compression are essentially the same.

Westinghouse has concluded that the PAD 4.0 Creep Model [
]^{a,c} at which the Vogtle capsules operate. However, the PAD 4.0 Creep Model provides acceptable results in the high temperature region, which is typically limiting for fuel performance analyses. Additional fuel rod creep data are presented for comparison with the PRXA **Optimized ZIRLO** creep model predictions.

Since there is essentially no difference in the key performance parameters (other than waterside corrosion) between Standard ZIRLO material and PRXA **Optimized ZIRLO** material up to the burnups achieved in these programs, the existing fuel performance models remain applicable for **Optimized ZIRLO** fuel rods up to the licensed fuel burnup limit (60 and 62 GWD/MTU for Combustion Engineering and Westinghouse fuel designs, respectively). NRC SER Conditions 6 and 7 have been satisfied.

---

* **Optimized ZIRLO™** and ZIRLO® are trademarks or registered trademarks of Westinghouse Electric Company LLC, its affiliates and/or its subsidiaries in the United States of America and may be registered in other countries throughout the world.

Table of Contents

1.0 Introduction

This report is being provided to address Conditions 6 and 7 of Section 5.0 of the SER to topical report WCAP-12610-P-A & CENPD-404-P-A Addendum 1-A (Reference 1) to provide **Optimized ZIRLO** LTA and creep/growth data. The data demonstrate that the current approved fuel performance models remain applicable for **Optimized ZIRLO** fuel rods.

Condition 6 of the SER to Reference 1 states the following:

6. "The licensee is required to ensure that Westinghouse has fulfilled the following commitment: Westinghouse shall provide the NRC staff with a letter(s) containing the following information (Based on the schedule described in response to RAI #3):
   a. Optimized ZIRLO™ LTA data from Byron, Calvert Cliffs, Catawba, and Millstone.
      i. Visual
      ii. Oxidation of fuel rods
      iii. Profilometry
      iv. Fuel rod length
      v. Fuel assembly length
   b. Using the standard and Optimized ZIRLO™ database including the most recent LTA data, confirm applicability with currently approved fuel performance models (e.g., measured vs. predicted).

   Confirmation of the approved models' applicability up through the projected end of cycle burnup for the Optimized ZIRLO™ fuel rods must be completed prior to their initial batch loading and prior to the startup of subsequent cycles. For example, prior to the first batch application of Optimized ZIRLO™, sufficient LTA data may only be available to confirm the models' applicability up through 45 GWd/MTU. In this example, the licensee would need to confirm the models up through the end of the initial cycle. Subsequently, the licensee would need to confirm the models, based upon the latest LTA data, prior to re-inserting the Optimized ZIRLO™ fuel rods in future cycles. Based upon the LTA schedule, it is expected that this issue may only be applicable to the first few batch implementations since sufficient LTA data up through the burnup limit should be available within a few years."

Condition 7 of the SER to Reference 1 states the following:

7. "The licensee is required to ensure that Westinghouse has fulfilled the following commitment: Westinghouse shall provide the NRC staff with a letter containing the following information (Based on the schedule described in response to RAI #11):
   a. Vogtle growth and creep data summary reports.
   b. Using the standard ZIRLO™ and Optimized ZIRLO™ database including the most recent Vogtle data, confirm applicability with currently approved fuel performance

models (e.g., level of conservatism in W rod pressure analysis, measured vs. predicted, predicted minus measured vs. tensile and compressive stress).

Confirmation of the approved models' applicability up through the projected end of cycle burnup for the Optimized ZIRLO™ fuel rods must be completed prior to their initial batch loading and prior to the startup of subsequent cycles. For example, prior to the first batch application of Optimized ZIRLO™, sufficient LTA data may only be available to confirm the models' applicability up through 45 GWd/MTU. In this example, the licensee would need to confirm the models up through the end of the initial cycle. Subsequently, the licensee would need to confirm the models, based upon the latest LTA data, prior to re-inserting the Optimized ZIRLO™ fuel rods in future cycles. Based upon the LTA schedule, it is expected that this issue may only be applicable to the first few batch implementations since sufficient LTA data up through the burnup limit should be available within a few years."

2.0 Condition 6 Compliance - LTA Data

2.1 LTA Program Schedule

The four listed LTA programs are complete. The Byron LTA program included both stress-relief annealed (SRA) and partially-re-crystallized annealed (PRXA) **Optimized ZIRLO** fuel rods while the other three LTA programs only included PRXA **Optimized ZIRLO** fuel rods. Table 1 summarizes the various LTA programs.

Table 1 – Optimized ZIRLO LTA Irradiation and Planned Examination Status

[ ]a,c

2.2 Data Presentation and Analysis

2.2.1 Visual Examination

Visual inspections were performed subsequent to each irradiation cycle in all of the LTA programs. A summary of the visual inspections from each of the LTA programs is described in the following subsections. In summary, no anomalous performance was observed.

Byron LTA

Visual inspections were performed on the Byron LTAs after each of the three irradiation cycles. Minor crud was reported on both SRA **Optimized ZIRLO** and Standard ZIRLO fuel rods at each inspection. No anomalies were reported for any of the alloys.

Calvert Cliffs LTA

The Calvert Cliffs LTA program is composed of [ ]^{a,c} assemblies each containing [ ]^{a,c} **Optimized ZIRLO** clad rods and [ ]^{a,c} ZIRLO clad rods. [ ]^{a,c} LTAs were inspected after 1 cycle of operation. Minor crud was observed on fuel rods, but no anomalies were observed. [ ]^{a,c} LTAs were inspected after 2 cycles of operation in the Calvert Cliffs Unit 2 plant. Minor crud was observed on fuel rods, but no anomalies were observed. [ ]^{a,c} LTAs were inspected after 3 cycles of operation in the Calvert Cliffs Unit 2 plant. Minor crud was observed on fuel rods, but no anomalies were observed. There were no areas of localized crud or corrosion accumulation. [ ]^{a,c} LTAs were inspected after 3 cycles of operation in the Calvert Cliffs Unit 1 plant. Minor crud was observed on fuel rods, but no anomalies were observed.

Catawba 1 LTA

The Catawba LTA program is composed of [ ]^{a,c} assemblies of the Westinghouse 17x17 Next Generation Fuel (NGF) design. [ ]^{a,c} LTAs were inspected after 1 cycle of operation in the Catawba Unit 1 plant. Dark crud was observed on the fuel rods and on many assembly components. The dark crud is thought to be due to the replacement of steam generators, consistent with the crud observed in the McGuire plants following steam generator replacement there. [ ]^{a,c} LTAs were inspected after 2 and 3 cycles of operation in the Catawba Unit 1 plant. A minor quantity of crud was observed on the fuel rods in the assemblies, but no anomalies were observed.

Millstone 3 LTA

The Millstone LTA program is composed of [ ]^{a,c} assemblies of the Westinghouse 17x17 NGF design. [ ]^{a,c} LTAs were inspected after 1 cycle of operation. Minor crud was observed on fuel rods in the NGF LTAs and in the Standard ZIRLO Robust Fuel Assembly (RFA) assemblies. No anomalies were observed. [ ]^{a,c} NGF LTAs were inspected after 2 cycles of operation in the Millstone Unit 3 plant. An expected normal quantity of non-adherent crud was observed on the fuel rods in the assemblies, but no anomalies were observed. [ ]^{a,c} NGF LTAs were inspected after 3 cycles of operation in the Millstone Unit 3 plant. The crud was [ ]^{a,c}.

2.2.2 Oxidation of Fuel Rods

Fuel rod oxide measurements have been made on the Byron, Catawba, Millstone, and Calvert Cliffs LTAs.

The oxide thickness from the Byron LTA program was measured after each cycle of operation. The oxide thickness from the Catawba, Millstone, and Calvert Cliffs LTA programs was measured after 2 and 3 cycles of operation. The data (Figures 1 and 2) show the corrosion rate of the **Optimized ZIRLO** fuel rods to be significantly lower relative to that of the Standard ZIRLO fuel rods.

Since the oxidation of **Optimized ZIRLO** material is well below the ZIRLO values, these data confirm the conservatism of using the ZIRLO model for corrosion calculations.

[ ] a,b,c

Figure 1 – Measured Oxide Thickness Plotted as a Function of the Modified Fuel Duty Index

Figure 2 – Measured Rod Peak Oxide Thickness Plotted as a Function of Rod Burn-Up

2.2.3 Profilometry

Fuel rod profilometry data is presented and discussed in Section 4.

2.2.4 Fuel Rod Length

Fuel rod length was measured on the Byron SRA **Optimized ZIRLO** fuel rods and the Byron, Catawba, Millstone, and Calvert Cliffs PRXA **Optimized ZIRLO** fuel rods. The measured fuel rod length is plotted with the Standard ZIRLO assembly average fuel rod growth data base in Figure 3. The measurements show the SRA and PRXA **Optimized ZIRLO** growth to be within the scatter band of the ZIRLO fuel rod growth data base.

[ ] a,b,c

Figure 3 – Growth Measurements from SRA and PRXA Optimized ZIRLO Fuel Rods

Shown in Figure 3 is the upper bound growth line used in shoulder gap calculations and the lower bound growth line used for rod internal pressure (RIP) uncertainty calculations in PAD 4.0. Based on the trends observed in the **Optimized ZIRLO** fuel rod growth, the design analyses for the shoulder gap closure and for the RIP calculations remain valid. In the post irradiation exams for fuel rod growth, no significant increase in shoulder gap has been observed. The trend is that the shoulder gap decreases with burnup. Therefore, the design evaluations for fuel rod to spacer grid engagement remain valid.

2.2.5 Fuel Assembly Length

Fuel assembly growth data are currently available from the Byron, Catawba, Millstone, and Calvert Cliffs programs. The assembly growths of the Zircaloy-4 (Calvert Cliffs) and **Optimized ZIRLO** LTAs are plotted in Figure 4 along with the Standard ZIRLO database. The comparison shows **Optimized ZIRLO** assemblies behave comparable to Standard ZIRLO and Zircaloy-4 assemblies.

[ ] a,b,c

Figure 4 – Assembly Growth Plotted as a Function of Fast Neutron Fluence

The fuel assembly growth trends are design specific. In Figure 5 the fuel assembly growth data for the 17x17 standard assembly designs are plotted along with the NGF LTA data and the upper bound, best estimate and lower bound growth curves. It can be observed in Figure 5 that the **Optimized ZIRLO** NGF LTA growth data is within the growth bounds. Therefore, the design calculations for fuel assembly growth remain valid.

Figure 5 -17x17 Standard Assembly Growth Plotted as a Function of Burnup

2.3 Summary

The LTA measurements showed the corrosion rate of the SRA **Optimized ZIRLO** fuel rods and PRXA **Optimized ZIRLO** fuel rods to be significantly lower than that of the Standard ZIRLO fuel rods and thus this property is bounded by the predictive capability of the current ZIRLO corrosion model. Similarly, the measured SRA/PRXA **Optimized ZIRLO** fuel rod growth is also within the predictive capability of the Standard ZIRLO fuel rod growth model as the measured values are well within the scatter band of the Standard ZIRLO fuel rod growth database. The measured **Optimized ZIRLO** fuel assembly growth is also within the scatter band of the Standard ZIRLO fuel assembly growth data base. Fuel rod profilometry data is presented and discussed in Section 4.

Based on these measurements and evaluations, the fuel rod and fuel assembly design calculations remain valid and the **Optimized ZIRLO** fuel will operate within design criteria.

3.0 Condition 7 Compliance - Creep/Growth Data

3.1 Creep/Growth Test Program Schedule and Status

The irradiation schedule of the Vogtle Creep/Growth tests that are needed to satisfy SER Condition 7 is shown in Figure 6. Test Assemblies A1, A2, A3 and A5 have all been discharged and all measurements and evaluations are complete for all of the discharged test assemblies. The data evaluation consists of laser outside diameter (OD) and length measurements, oxide thickness measurements, coolant temperature calculations based on the fuel assembly powers, determination of the gamma-heating rate, temperature and internal pressure calculations, and measurement of the fast flux by retrospective dosimetry.

Note that all stresses are based on standard thick-wall equations.

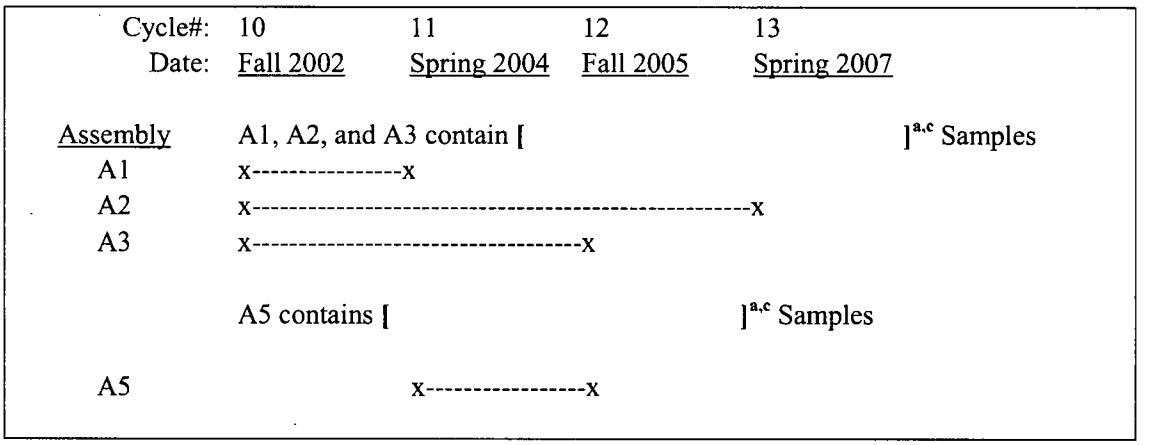

Figure 6 – Irradiation Schedule of the Creep/Growth Test

3.2 Creep/Growth Irradiation Conditions

The samples are located in segmented rods suspended inside the fuel assembly thimble tubes. All of the test samples are placed in positions approximately 90 cm above and below the core mid-plane at elevations between mid-grids or intermediate flow mixer grids. The samples are radially located relatively close to core center. The samples are always hosted by a one-cycle burned fuel assembly. Figure 7 presents the measured dosimetry data for Test Assembly A1 (irradiated for 1 cycle in cycle 10) from the rods numbered 2, 5, 8 and 11 which are located in each of the four fuel assembly faces at the mid-point. Figure 7 shows that the fast flux is constant radially and axially. Since there was no radial fast flux gradient, all subsequent measurements were only made on the faces closest and farthest from core center. Figures 7 to 10 show that the measured fast flux is constant radially and axially for [ ]a,c. Further, Figures 7 to 10 show that the average measured fast flux values for each test assembly are similar. The average measured values are [ ]a,c

[

]^{a,c}. This shows that the fast flux does not vary from cycle-to-cycle, and that the samples in each test assembly were irradiated at the same constant fast flux value. Further, the dosimetry measurements on these samples confirm calculations that showed no axial gradient in fast flux for the axial positions of the samples. As a result, the samples, which are located at different axial positions, can be considered to have been irradiated at the same flux level.

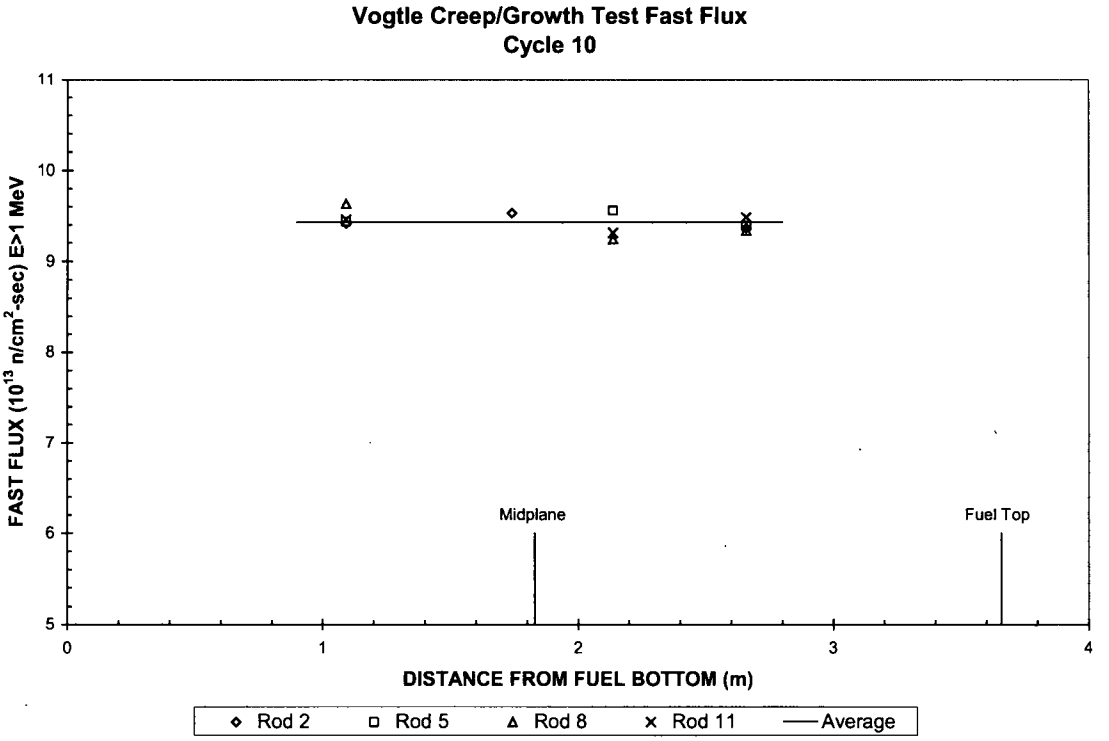

Figure 7 - Measured Fast Flux for Test Assembly A1 - 1 Cycle Irradiation

a,b,c

Figure 8 - Measured Fast Flux for Test Assembly A5 - 1 Cycle Irradiation

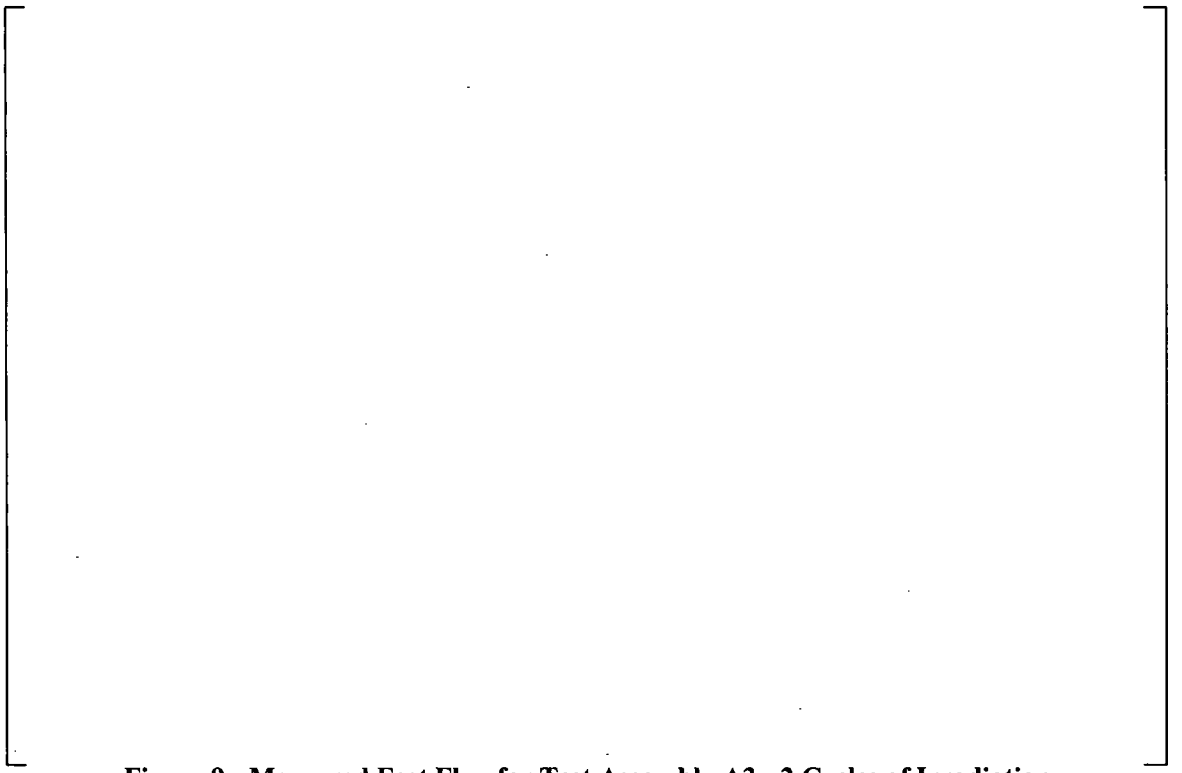

a,b,c

Figure 9 - Measured Fast Flux for Test Assembly A3 - 2 Cycles of Irradiation

[a,b,c

]

Figure 10 - Measured Fast Flux for Test Assembly A2 - 3 Cycles of Irradiation

The amount of gamma-heating was determined by testing and evaluating samples having the same tubing lot with two different internal heating rates. The samples did not contain any fuel. Each sample had either a solid cylinder or an internal tube to support the sample if collapse were to occur (the samples were tested at compressive stress levels that calculations showed would not result in collapse, and none of the examined samples have exhibited collapse). Since the mass of the solid cylinders was much greater than the internal tubes, these two different types of samples generated different amounts of internal heat due to gamma-heating. As a result, the gamma-heating was evaluated by parametric calculations using the diameter strain data. The gamma-heating was used to calculate the sample temperature distributions. The calculated average tube temperatures for Test Assemblies A1, A5, A3 and A2 were in the range of [ ]^{a,c}. The samples in the lowest axial positions are associated with average temperatures of [ ]^{a,c}, and the samples in the highest axial position are associated with average temperatures of [ ]^{a,c}.

3.3 Creep/Growth Test Data

The results to be presented are 1) the irradiation growth and irradiation creep of Standard ZIRLO and PRXA **Optimized ZIRLO** material and 2) the irradiation creep of Standard ZIRLO material under tensile and compressive deviatoric hoop stress components. The following presentation of the irradiation growth and irradiation creep data summarizes currently available Creep/Growth data.

The measurement accuracy associated with the OD and length laser micrometer measurements is excellent. The 95% confidence interval of the mean OD value is about [ ]^{a,c}. The

95% confidence interval measurement error is very small because the data for each sample consist of [

]^{a,b,c}.

The calculated fast fluence for Test Assemblies A1, A5, A3, and A2 is [ ]^{a,c} respectively. The Creep/Growth test does not contain fuel so the irradiation is properly characterized by fast fluence and not burnup.

3.3.1 Irradiation Growth

Figures 11, 12, and 13 present the diameter irradiation growth data for Standard ZIRLO, PRXA **Optimized ZIRLO** and SRA **Optimized ZIRLO** tubes fabricated by a [ ]^{a,c} 4-pass tube reduction sequence from TREX to final size tubing. The irradiation growth samples had holes to allow the coolant water to be both at the OD and ID. This insured that the samples were unstressed. Each marker in Figures 11, 12, and 13 represents one sample. The strain scale was selected to present the 1- , 2- and 3-cycle data using the same range. Irradiation growth data are available for two PRXA **Optimized ZIRLO** lots with different tin contents. Figures 11, 12, and 13 show that the irradiation growth of SRA Standard ZIRLO and PRXA **Optimized ZIRLO** are similar.

[a,b,c]

Figure 11 - ZIRLO Irradiation Growth after 1 Cycle (Test Assembly A1).

Figure 12 - ZIRLO Irradiation Growth after 2 Cycles (Test Assembly A3)

Figure 13 - ZIRLO Irradiation Growth after 3 Cycles (Test Assembly A2)

3.3.2 Irradiation Creep

The irradiation creep was measured using samples filled with helium gas. The internal gas pressure was either below or above system pressure so that the samples were in either compressive or tensile hoop stress, respectively. The irradiation creep diameter strain, $\Delta D/D_o(ic)$, was calculated from the total measured strain, $\Delta D/D_o(total)$, and the average irradiation growth strain, $\Delta D/D_o(ig)$, according to,

$$\Delta D/D_o(ic) = \Delta D/D_o(total) - \Delta D/D_o(ig)$$

Figures 14 to 17 present the diameter irradiation creep data for Standard ZIRLO, PRXA **Optimized ZIRLO** (tube samples from two lots with different tin contents) and SRA **Optimized ZIRLO** tubes fabricated by a [ ]^{a,c} 4-pass tube reduction sequence from TREX to final size tubing. Each marker in Figures 14 to 17 represents one sample. The irradiation creep of all of the materials is similar based on sample-to-sample variability. This shows that the irradiation creep of PRXA **Optimized ZIRLO** and SRA Standard ZIRLO material are similar. Figure 14 presents the 1-cycle data. Figure 15 presents the 2-cycle data. Figures 16 and 17 present the 3-cycle data. Note that the 3-cycle data are available for two different deviatoric hoop stress component values.

The irradiation creep strain at a deviatoric hoop stress component of about [ ]^{a,c} is significantly larger than the diameter irradiation growth strain. Comparison of Figure 14 with Figure 11 for 1 cycle of irradiation, Figure 15 with Figure 12 for two cycles of irradiation, and Figure 16 with Figure 13 for 3 cycles of irradiation (note the difference in the strain scales between Figures 11 to 13 versus Figures 14 to 16) shows that the irradiation growth of PRXA **Optimized ZIRLO** and Standard ZIRLO material is about an order of magnitude less than the irradiation creep for a deviatoric hoop stress component of about [ ]^{a,c}.

a,b,c

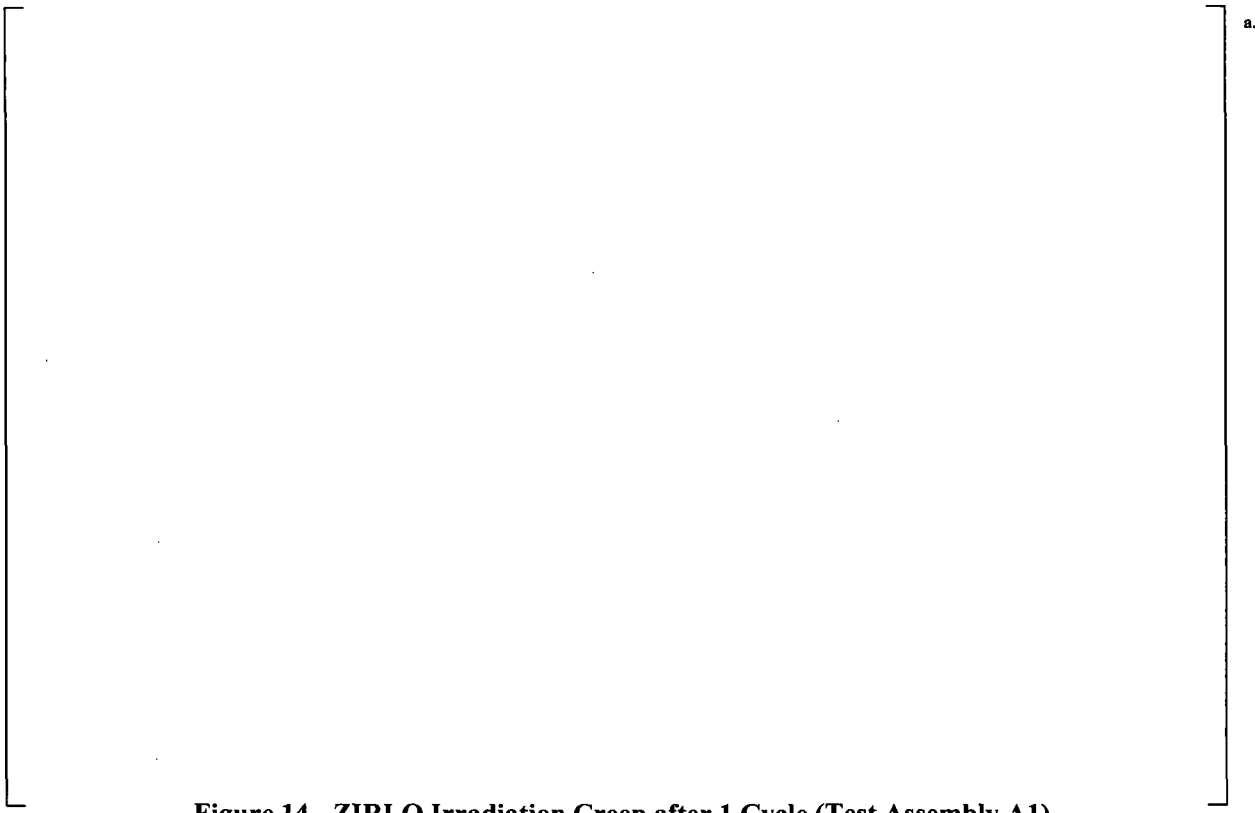

Figure 14 - ZIRLO Irradiation Creep after 1 Cycle (Test Assembly A1).

a,b,c

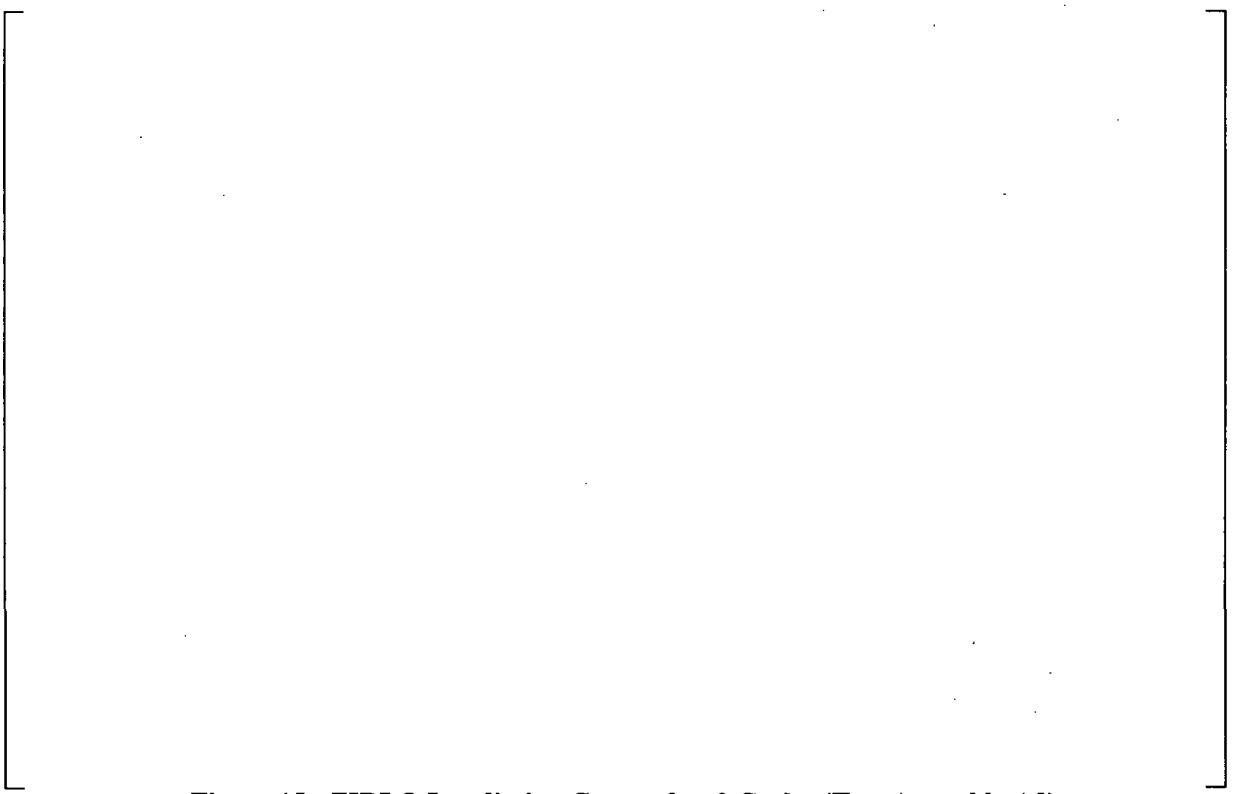

Figure 15 - ZIRLO Irradiation Creep after 2 Cycles (Test Assembly A3)

Figure 16 - ZIRLO Irradiation Creep for 3 Cycles (Test Assembly A2)

Figure 17 - ZIRLO Irradiation Creep after 3 Cycles (Test Assembly A2)

Figures 18 to 21 present an evaluation of the Standard ZIRLO irradiation creep data for tensile and compressive deviatoric hoop stress components. The tension versus compression data are presented as a function of the deviatoric hoop stress component instead of hoop stress because the driving force for plastic deformation, which includes irradiation creep, is the deviatoric hoop stress component. The total hoop stress is the sum of the deviatoric and hydrostatic stress components. The hydrostatic component does not produce plastic deformation.

The data in Figures 18 to 21 cover deviatoric hoop stress component ranges from [ ]^{a,b,c}. This deviatoric hoop stress component range approximately envelopes the range of hoop stresses experienced by fuel rods during normal operation. Each marker in Figures 18 to 21 represents one sample. Most of the stress levels include duplicate samples to confirm strain level consistency. Figures 18 to 21 show that the scatter of duplicate samples is negligible. Furthermore, Figures 18 to 21 show that the data are very consistent between stress levels, the strain behavior is linear as a function of the deviatoric hoop stress component, and the regression fits to the data approximately exhibit zero strain when the deviatoric hoop stress component is zero, demonstrating that compressive and tensile creep are equivalent.

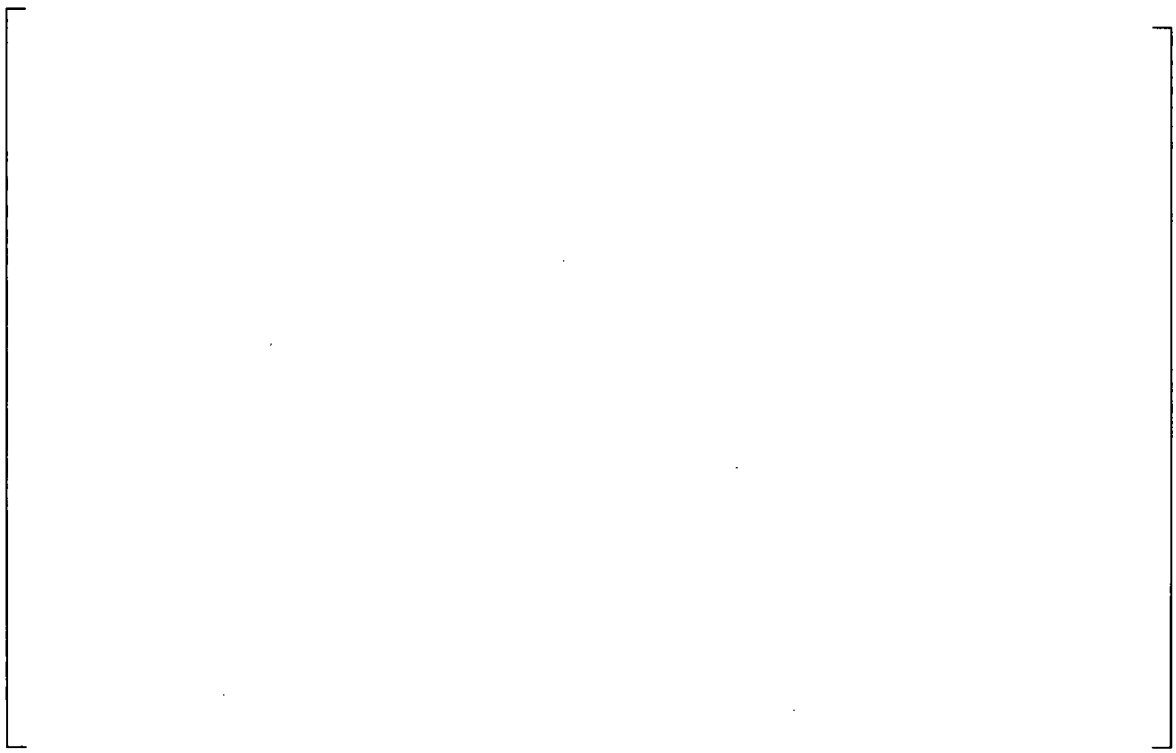

Figure 18 - Irradiation Creep in Tension and Compression after 1 Cycle (Test Assembly A1)

[ ] a,b,c

Figure 19 - Irradiation Creep in Tension and Compression after 1 Cycle (Test Assembly A5)

[ ] a,b,c

Figure 20 - Irradiation Creep in Tension and Compression after 2 Cycles (Test Assembly A3)

[a,b,c

]

Figure 21 - Irradiation Creep in Tension and Compression after 3 Cycles (Test Assembly A2)

3.4 Discussion of the OD Strain Components

Figures 18 to 21 present the SRA Standard ZIRLO irradiation creep strain for compressive and tensile deviatoric hoop stress components. The Creep/Growth data cannot be used to determine the fluence associated with the transition from the transient component to the steady state component because the 1-cycle Vogtle Creep/Growth fluence level occurs after this transition. However, Halden measurements on SRA Standard ZIRLO samples are available (IFA-663 and IFA-617) that allow the determination of this transition fluence. The duration of the transient component is,

298 full power hours (FPH) at a flux of 2.7×10^{13} n/cm^2-s (E>1) for Halden Test IFA-663, and
243 FPH at a flux of 4.5×10^{13} n/cm^2-s (E>1) for Halden Test IFA-617.

In terms of fluence, the average duration of the transient is,

2.7×10^{13} n/cm^2-s x 298 h x 3600 s/h = 0.029×10^{21} n/cm^2
4.5×10^{13} n/cm^2-s x 243 h x 3600 s/h = $\underline{0.039 \times 10^{21}\ \text{n/cm}^2}$
0.034×10^{21} n/cm^2 average

The calculated fluences for the Creep/Growth test assemblies are [

]^{a,c}

[

]^{a,c}

Based on the Halden data, the Creep/Growth samples are in steady state creep for [ ]^{a,c} of their irradiation period. Therefore, a significant fraction of the total irradiation creep strains presented in Figures 18 to 21 is steady state irradiation creep.

The diameter strain magnitude of the transient and steady state irradiation creep components may be determined using the Vogtle Creep/Growth data. Figures 18 to 21 show that the regression fits may be used to represent the data because the data scatter relative to the regression fit is very small. The regression fits were used to calculate the irradiation creep strains in tension and compression for deviatoric hoop stress components [ ]^{a,c} (see Figure 22). The irradiation creep rates were calculated based on these strain values. Figure 22 shows that the data are in steady state creep, and that ZIRLO material exhibits both transient and steady state irradiation creep components. The diameter steady state creep rate component is illustrated by the linear strain versus fluence behavior for 3 cycles. The transient component is shown by the strain intercept at zero fluence. Note that the Vogtle cycle fluence levels are higher than the duration of the transient component so that the transient component has saturated after one cycle. Further, Figure 22 shows that the steady state irradiation creep rate in tension is about the same as in compression.

According to the original reported evaluation of Halden test IFA-585 (Reference 2), the steady state irradiation creep rate in tension was 50% higher than in compression. However, the original evaluation has been updated in Reference 3 to correct for the effects of oxide thickness. If the updated IFA-585 data are evaluated using the deviatoric hoop stress component correlation, the result shows that the deviatoric stress component represents a more appropriate reflection of the data than the (total) hoop stress. This confirms that the driving force for irradiation creep is the deviatoric hoop stress component.

[ ] a,b,c

Figure 22 - Fluence Dependence of ZIRLO Irradiation Creep in Tension and Compression

4.0 Comparison of Profilometry Data with Predictions

Evaluations of the measured creep and growth data from the completed ZIRLO and **Optimized ZIRLO** irradiation programs have been performed and are described in Section 3. The purpose of this section (Section 4.0) is to describe analytical evaluations relating the measured Vogtle Creep/Growth test data and other ZIRLO creep and growth profilometry data to the Westinghouse licensed fuel performance models (PAD 4.0 and FATES3B). The intent is to assess the ability of the existing creep models to predict the data. ZIRLO models in PAD 4.0 are incorporated into FATES3B. Therefore, any conclusions about creep and growth predictions using PAD 4.0 are applicable to creep and growth predictions using FATES3B.

4.1 Introduction

The Westinghouse LTA programs described in Section 2.0 are intended to provide data on the ZIRLO and **Optimized ZIRLO** cladding performance in-reactor. The LTA programs provide data for prototypical fuel rod designs. The Vogtle Creep/Growth test described in Section 3 was designed to determine whether the fuel rod cladding creep response under a tensile stress is equivalent in magnitude to the creep response under compressive stress. Consequently, a broad range of clad pressure differentials were tested, with temperature differences minimized. The use of non-fueled specimens (capsules) results in specimen temperatures close to that of the coolant at the mid-plane elevation in the core. With no fuel present, there is an insignificant temperature gradient across the cladding and coolant film, so the specimen temperatures are [ ] [a,c] lower than fuel clad average temperatures for typical fuel rod conditions (see Figure 27). The design of the Vogtle Creep/Growth capsules allowed individual capsule-to-capsule variations in stress to be tightly controlled under constant temperature and fast flux, and to maintain nearly constant stress during the irradiation. The strains were accurately measured, enabling tensile and compressive creep behavior to be clearly separated. Accurate tensile stresses are not possible to determine within a fuel rod due to the uncertainty associated with pellet-clad contact. Accumulated diametral strain was measured for each capsule at the end of one, two, and three cycles of exposure for the Vogtle samples.

Note that in the case of the Vogtle Creep/Growth test data, the graphs comparing predicted diameter changes using the PAD 4.0 and STAV models to measured diameter changes are creep diameter changes (that is, for the gas pressurized samples, the total measured strain minus irradiation growth). In the case of the LTA fuel rods, the graphs present the total diameter change i.e., as-fabricated diameter minus measured diameter profiles at poolside or hot cell, and positive is directed inward. Vogtle Creep/Growth strains use the conventional mechanical definition that positive is directed outward.

4.2 Review of ZIRLO and Optimized ZIRLO Creep Measurements

The following sections describe creep measurements and predictions for Vogtle Creep/Growth ZIRLO and **Optimized ZIRLO** capsule specimens, Byron **Optimized ZIRLO** fuel rods, and Calvert Cliffs, Millstone 3, and Catawba 1 **Optimized ZIRLO** fuel rods. Additional measurements and predictions are also provided for Plant A ZIRLO and Plant B **Optimized ZIRLO** fuel rods which are pertinent, but were not part of the test programs referenced in the **Optimized ZIRLO** SER.

4.2.1 Calvert Cliffs Creep Measurements

Profilometry measurements were performed on [ ]^{a,c} from a Calvert Cliffs' 2-cycle assembly. The results were as expected for a fuel rod operating in fuel-clad contact for some time. The diameters appeared to be recovered to near nominal as-fabricated with a maximum diameter of [ ]^{a,c} and a minimum diameter of [ ]^{a,c}. Because the measurements were made after 2 cycles of irradiation, significant pellet-clad contact was quite likely.

4.2.2 Millstone Creep Measurements

Profilometry measurements were performed on [ ]^{a,c} from four Millstone 3 3-cycle assemblies. The results were as expected for a fuel rod operating in fuel-clad contact for some time. The maximum rod outside diameters ranged from [ ]^{a,c}.

4.2.3 Catawba Creep Measurements

Profilometry measurements were performed on [ ]^{a,c} from two Catawba 1 3-cycle assemblies. The results were as expected for a fuel rod operating in fuel-clad contact for some time. The maximum rod outside diameters ranged from [ ]^{a,c}.

4.2.4 Vogtle Creep Measurements

The PAD 4.0 Creep Model equations for irradiation creep and in-reactor thermal creep were used to provide PAD 4.0 Creep Model predictions for comparison to the Vogtle Creep/Growth data. The capsule tubes are free standing because of the relatively large gap in the capsule between the outer capsule tube inside diameter and the inner mandrel outside diameter. The measured diameter strains presented in Section 3 are shown in Figure 23 plotted against the PAD 4.0 Creep Model predictions.

Figure 23 shows that the PAD 4.0 Creep Model [ ]^{a,c} the Vogtle Creep/Growth capsule diameter strain data. The diameter strain [ ]^{a,c} is primarily due to PAD 4.0 Creep Model temperature extrapolations that are required to predict the Vogtle Creep/Growth test which was irradiated at relatively [ ]^{a,c}. Strain predictions in Figure 23 have also been made for the Vogtle Creep/Growth capsules using the STAV Model described in Reference 4. The STAV Model irradiation creep and in-reactor thermal creep equations were coded into a spreadsheet in order to provide STAV Model predictions for comparison with the Vogtle Creep/Growth data. The STAV Model is NRC approved for Westinghouse BWRs, and contains PWR verification data using Zircaloy-4 cladding. The STAV ZIRLO Model has a [ ]^{a,c} than the PAD 4.0 and FATES3B Creep Models. ZIRLO irradiation creep was modeled in the STAV Model using [ ]^{a,c} on Zircaloy-4 creep as described in Reference 5. Figure 23 shows that the STAV Model does a reasonable job predicting the Vogtle Creep/Growth capsule diameter strains but over-predicts the data slightly over the full range in clad stress as shown in Figure 23. The STAV Model predictions were added to demonstrate that a creep model with a [ ]^{a,c} can adequately predict the low temperature data. The applicability of PAD 4.0 Creep Model predictions at the limiting high temperature region is discussed in Section 4.3.

[ ]^{a,b,c}

Figure 23 - PAD 4.0 and STAV Predictions for the Measured Vogtle Specimens

4.2.5 Plant A Creep Measurements

Plant A ZIRLO data was used to calibrate PAD 4.0 and is discussed here for comparison. Both PAD 4.0 and STAV predictions of the Plant A ZIRLO fuel rod profilometry data are acceptable. The predicted profilometry (diametral change) measurements are plotted against PAD 4.0 and STAV predictions for the [ ]^{a,c} rods originally used to calibrate PAD 4.0 in Figure 24. PAD 4.0 was calibrated with the Plant A data and is, therefore, best-predicted on average. STAV was calibrated to a different data set. The clad temperatures for the Plant A data points ranged from [ ]^{a,c} versus [ ]^{a,c} for the Vogtle Creep/Growth samples. The portion of the fuel rod which is [ ]^{a,c} is the hot upper region. This can be seen more clearly in Section 4.3 Figure 28.

[ ] a,b,c

Figure 24 - PAD 4.0 and STAV Predictions of the Plant A Calibration Data

4.2.6 Byron Creep Measurements

Westinghouse discovered an uncertainty in the fast fluence data in the prior analysis of the Byron **Optimized ZIRLO** LTA profilometry data given in Reference 6. This uncertainty was due to the low power level related to the non-limiting location of the Byron LTA rods, and that the Byron LTA contained fuel rods with [ ]^{a,c} which reduced fast flux and clad temperatures relative to typical fuel rods in the core. Therefore, the power level and fast flux that the [ ]^{a,c} LTA fuel rods experienced was significantly less than the assembly average. The fast flux level in the prior analysis was not reduced to reflect the lower power level of the measured LTA fuel rods.

The Byron LTA fast flux has been corrected and the [ ]^{a,c} Byron rods have been analyzed again with PAD 4.0. The Byron rods were also analyzed with the STAV Model. The profilometry results are shown in Figure 25. As expected, the reduction in fast flux results in a reduction in the PAD 4.0 predicted creep diameter strain. The Byron strain rates are now [ ]^{a,c}, similar to the Vogtle Creep/Growth strain rates. This behavior is primarily due to the similarity in Byron and Vogtle clad temperatures. The STAV results are also shown on Figure 25. STAV does a reasonable job of predicting the [ ]^{a,c} profilometry. The acceptability of PAD 4.0 Model predictions at the limiting high temperature region is discussed in Section 4.3.

Figure 25 - PAD 4.0 and STAV Predictions of the Byron Profilometry (with Corrected Fluence)

4.2.7 Plant B Creep Measurements

New diameter measurements are available from Westinghouse **Optimized ZIRLO** fuel in Plant B and are also presented here for comparison. Profilometry data was obtained for [ ]^{a,c} fuel rods, [ ]^{a,c} ZIRLO fuel rod and [ ]^{a,c} **Optimized ZIRLO** fuel rod, and analyzed with both PAD 4.0 and STAV. Comparisons between PAD 4.0 and STAV predictions and the measured data are shown in Figure 26. The PAD 4.0 and STAV models [ ]^{a,c} the measurements about the same amount on average. In this case, the hot upper region of the Plant B fuel rod is best-predicted. This can best be seen in the axial distribution plot in Section 4.3 Figure 29.

Figure 26 – PAD 4.0 and STAV Diameter Predictions for Plant B

4.3 Additional Validation of ZIRLO and Optimized ZIRLO Creep

The cladding temperature associated with each data point from Figures 23 through 26 is plotted against the fluence of the data points as shown in Figure 27. The Vogtle, Plant A, Byron, and Plant B data are plotted. Figure 27 demonstrates how the non-fueled Vogtle data and the [ ]^{a,c} Byron data differ from typical fuel rod data represented by Plant A and Plant B. The Vogtle temperatures are [ ]^{a,c} and the accumulated fluence in the Vogtle specimens is [ ]^{a,c}. The Byron temperatures are also [ ]^{a,c} as explained in Section 4.2.3.

Figure 27 shows the in-life cladding temperature distribution over the length of the fuel rod for all of the rods in each of four data sets. For a given fuel rod, the temperature at each end of the rod is lower than the temperature in the upper section. The temperature distribution forms a vertical loop on the graph. Since the internal pressure does not vary over the rod length, the maximum cladding creep rate will always occur at the maximum temperature. Therefore it is important to show that the hot upper section of the fuel rod is well predicted. The axial profilometry measurements are compared to predicted diameter changes in Figures 28 and 29 for Plant A and Plant B, respectively. The PAD 4.0 creep model provides acceptable results in the high temperature region in Figures 28 and 29, which is typically limiting for fuel performance analyses.

[ ]^{a,b,c}

Figure 27 - In-life Temperature Versus Fluence

Figure 28 - Axial Distribution of Measured Creep with PAD 4.0 and STAV Predictions - Plant A

Figure 29 - Axial Distribution of Measured Creep with PAD 4.0 and STAV Predictions - Plant B

5.0 Conclusions

Visual examinations of the LTA fuel rods indicate excellent performance. While there was some minor crud observed on some of the rods, there were no anomalies observed. Measurements of clad waterside corrosion, fuel rod axial growth and assembly axial growth also indicate excellent performance. The **Optimized ZIRLO** performance in these areas is significantly better than earlier Westinghouse Zircaloy-4 cladding. Oxidation and growth are reduced. Brief descriptions of these LTA programs and comparisons of the measurements with other Westinghouse cladding materials are provided in Section 2.0. Section 2.0 satisfies the requirements of SER Condition 6.

Additional ZIRLO and **Optimized ZIRLO** diameter profiles over the rod lengths were included in the measurements to assess the creep behavior of these cladding alloys. Diameter profile data is used from Vogtle. The Vogtle Creep/Growth tests were designed to provide comparisons between the ZIRLO material and the **Optimized ZIRLO** material under well-controlled stress, flux, and temperature conditions. The data support the Westinghouse conclusions that the difference between ZIRLO and **Optimized ZIRLO** irradiation creep is insignificant. Furthermore, the data clearly show that the creep in tension and creep in compression are equivalent. Section 3.0 provides details of the evaluations of the Vogtle creep strain measurements.

An effort was initiated to understand the Vogtle non-fueled capsule data. Previous calibration data (Plant A), Byron data, and new data (Vogtle and Plant B) were re-examined in detail. It was concluded that the ZIRLO creep model [ ]^{a,c}; however, the creep model is acceptable at higher temperatures where the model is calibrated and applied in design. Sections 3.0 and 4.0 satisfy SER Condition 7.

Compliance with NRC Conditions 6 and 7 of Section 5.0 of the SER to the **Optimized ZIRLO** topical report WCAP-12610-P-A & CENPD-404-P-A Addendum 1-A (Reference 1), is demonstrated in this report up to the licensed fuel burnup limit (60 and 62 GWD/MTU for Combustion Engineering and Westinghouse fuel designs, respectively).

6.0 References

1. WCAP-12610-P-A & CENPD-404-P-A Addendum 1-A, "Optimized ZIRLO™," July 2006.
2. M. McGrath, "In-Reactor Creep Behavior of Zircaloy Cladding," International Topical Meeting on Light Water Reactor Fuel Performance, American Nuclear Society, Park City Utah, April 10-13, 2000.
3. J. Foster and M. McGrath, "In-Reactor Creep Behavior of Zircaloy Cladding," International Topical Meeting on Light Water Reactor Fuel Performance, American Nuclear Society, San Francisco CA, September 30-October 3, 2007.
4. WCAP-15836-P-A, "Fuel Rod Design Methods for Boiling Water Reactors – Supplement 1 Volume 1," April 2006.
5. WCAP-12610-P-A, "VANTAGE+ Fuel Assembly Reference Core Report," April 1995.
6. Letter from J. A. Gresham (Westinghouse) to U.S. Nuclear Regulatory Commission, "SER Compliance with WCAP-12610-P-A & CENPD-404-P-A Addendum 1-A "Optimized ZIRLO™," LTR-NRC-07-58 Rev. 1, February 5, 2008.